Fuel 315 (2022) 123097

Contents lists available at ScienceDirect

Fuel

journal homepage: www.elsevier.com/locate/fuel

Full Length Article

Versatile Ni-Ru catalysts for gas phase CO_2 conversion: Bringing closer dry reforming, reverse water gas shift and methanation to enable end-products flexibility

Loukia-Pantzechroula Merkouri [a,*], Estelle le Saché [a], Laura Pastor-Pérez [a,b], Melis S. Duyar [a], Tomas Ramirez Reina [a,b,*]

[a] Department of Chemical and Process Engineering, University of Surrey, Guildford GU2 7XH, UK
[b] Department of Inorganic Chemistry and Materials Sciences Institute, University of Seville-CSIC, 41092 Seville, Spain

ARTICLE INFO

Keywords:
CO_2 recycling
Dry Reforming of Methane
Reverse Water-Gas Shift
CO_2 methanation
Ni-Ru bimetallic catalyst

ABSTRACT

Advanced catalytic materials able to catalyse more than one reaction efficiently are needed within the CO_2 utilisation schemes to benefit from end-products flexibility. In this study, the combination of Ni and Ru (15 and 1 wt%, respectively) was tested in three reactions, i.e. dry reforming of methane (DRM), reverse water–gas shift (RWGS) and CO_2 methanation. A stability experiment with one cycle of CO_2 methanation-RWGS-DRM was carried out. Outstanding stability was revealed for the CO_2 hydrogenation reactions and as regards the DRM, coke formation started after 10 h on stream. Overall, this research showcases that a multicomponent Ni-Ru/CeO_2-Al_2O_3 catalyst is an unprecedent versatile system for gas phase CO_2 recycling. Beyond its excellent performance, our switchable catalyst allows a fine control of end-products selectivity.

1. Introduction

Climate change is a major challenge faced by the entire global community. Greenhouse gas (GHG) emissions continue to rise due to anthropogenic activities. In particular, carbon dioxide (CO_2) emissions are the most alarming ones due to the global dependency on fossil fuels [1]. In 2019, the power sector itself accounted for 36% of the global CO_2 emissions [2]. It is estimated that CO_2 is responsible for 60% of the global warming effects [3]. Its average monthly recorded concentration in September 2021 was 413 ppm, the highest ever [4]. One solution is carbon capture and storage (CCS) [1,5], but CO_2 utilisation is another attractive solution as it addresses the issue of resource depletion by using CO_2 as a carbon pool, eventually producing valuable chemicals and fuels [6–8].

There are various commercialised applications for utilising CO_2 to produce higher value chemicals such as urea, carboxylic acids, and isocyanates [9]. One emerging approach is the production of syngas, which in turn can be converted into higher hydrocarbons via Fischer-Tropsch synthesis [9–12]. CO_2 can also be converted directly to synthetic natural gas (methane), which can enable large scale renewable energy storage through Power-to-Gas schemes [13–15]. Herein we focus on the conversion of CO_2 into syngas via dry reforming of methane (DRM) (1), carbon monoxide (CO) via reverse water–gas shift reaction (RWGS) (2), and synthetic natural gas (SNG), i.e. methane (CH_4), via CO_2 methanation reaction (3). These reactions are presented below [16].

$$CO_2 + CH_4 \leftrightarrow 2CO + 2H_2 \quad \Delta H^{\circ}_{298K} = +247\ kJ.mol^{-1} \tag{1}$$

$$CO_2 + H_2 \leftrightarrow CO + H_2O \quad \Delta H^{\circ}_{298K} = +41\ kJ.mol^{-1} \tag{2}$$

$$CO_2 + 4H_2 \leftrightarrow CH_4 + 2H_2O \quad \Delta H^{\circ}_{298K} = -165\ kJ.mol^{-1} \tag{3}$$

DRM produces syngas using the two most abundant greenhouse gases, CO_2 and CH_4. The H_2/CO ratio of the produced syngas is lower than the stoichiometric 1:1, because of the simultaneous occurrence of the RWGS reaction. The low ratio from DRM is more suitable for long chain hydrocarbon production via Fischer-Tropsch (FT) synthesis [10,17,18] and as a result, DRM has attracted attention recently [10,17,19–24]. RWGS is of interest, especially for fixing the syngas ratio in various applications and when combined with other processes, such as the FT synthesis and CAMERE process, which produce hydrocarbons and methanol, respectively [12,25,26]. More specifically, the combination of the RWGS and the methanol synthesis in the so-called CAMERE

* Corresponding authors at: Department of Chemical and Process Engineering, University of Surrey, Guildford GU2 7XH, UK (T. Ramirez Reina).
E-mail addresses: l.merkouri@surrey.ac.uk (L.-P. Merkouri), t.ramirezreina@surrey.ac.uk (T. Ramirez Reina).

https://doi.org/10.1016/j.fuel.2021.123097
Received 27 October 2021; Received in revised form 22 December 2021; Accepted 29 December 2021
Available online 13 January 2022

process leads to higher methanol production [27–30]. CO_2 hydrogenation to methane, which is also referred to as synthetic natural gas (SNG), using H_2 from renewable energy driven water electrolysis is known as Power-to-Gas technology. Power-to-Gas schemes are appealing as a large scale storage option for renewable electricity produced in excess of demand [14,31–33].

As high temperatures are needed for the endothermic reactions, catalysts are prone to deactivation via sintering [21,34]. Even for the exothermic CO_2 methanation reaction, the development of hot spots may occur thus deactivating the catalysts through thermal sintering [35,36]. Carbon deposition is another major culprit while these reactions are carried out because the active sites of the catalyst are covered [18]. Coking of the catalysts occurs because of some side reactions, i.e. Boudouard, CO and CO_2 reduction, and CH_4 decomposition (4–7), that take place simultaneously and influence the catalytic performance [16,18,34,37].

$$2CO \leftrightarrow C + CO_2 \quad \Delta H^{o}_{298K} = -171 \text{ kJ.mol}^{-1} \tag{4}$$

$$CO + H_2 \leftrightarrow C + H_2O \quad \Delta H^{o}_{298K} = -131.3 \text{ kJ.mol}^{-1} \tag{5}$$

$$CO_2 + 2H_2 \leftrightarrow C + 2H_2O \quad \Delta H^{o}_{298K} = -90 \text{ kJ.mol}^{-1} \tag{6}$$

$$CH_4 \leftrightarrow C + 2H_2 \quad \Delta H^{o}_{298K} = +75 \text{ kJ.mol}^{-1} \tag{7}$$

Among the different active phases, Ni is the most frequently studied metal due its low cost and high activity in the DRM [18,38,39], in the RWGS [40–42] and in the CO_2 methanation [43–45]. Ni is prone to deactivation due to the formation of coke and sintering and alternatives are needed to boost the catalytic performance [46]. Noble metals, such as ruthenium (Ru), rhodium (Rh), palladium (Pd), and platinum (Pt), have shown high activity and stability as well as resistance to sintering and carbon formation in the DRM [18,47,48], in the RWGS [49,50] and in the CO_2 methanation [51,52]. Ru especially is the most active CO_2 methanation catalyst [53] and it is the cheapest noble metal (Ru = 22.2€/g, Rh = 530.7€/g, Pd = 69.8€/g, Pt = 29.6€/g on 1 Sept. 2021) [54]. A synergistic effect has been achieved in prior reports upon combining Ni and Ru, which resulted in increased Ni dispersion, enhanced performance and lower Ru loading [31,55,56].

In terms of supports and promoters, cerium oxide (CeO_2) has been extensively studied as a support in reforming [19,38,57] and hydrogenation reactions [49,58,59], due to its excellent oxygen storage capacity. CeO_2 forms oxygen vacancies, helping the oxidation of carbon [57,60,61]. CeO_2-Ni interfaces in particular have been shown to facilitate activation of CO_2 [62]. CeO_2 has a low specific surface area which can be improved by combination with aluminium oxide (Al_2O_3) [57], due to the latter's high specific surface area which can improve metal dispersion [22,63]. However, its increased acidity enhances coke formation and sintering [22]. Consequently, the combination of CeO_2 and Al_2O_3 is a promising support since the result is a high specific surface area basic material. The addition of CeO_2 into an Al_2O_3-supported catalyst used in the DRM, the RWGS and the CO_2 methanation reactions separately, enhances its activity and stability, promotes the oxidation of carbon deposits and increases the active metal dispersion, while extending the catalyst's lifetime due to its excellent redox properties [19,38,42,57,60,64]. $Ce_{0.5}Zr_{0.5}O_2$ has reported resistance to sintering at elevated temperatures, and a remarkable oxygen accessibility and mobility on the surface [21,31,44,61]. Characteristically, this support has oxygen bulk diffusion two times higher than ceria itself hence leading to an enhanced oxygen storage and an increased efficiency in the redox reactions of ceria [61].

While these reactions are often treated separately, CO_2 activation forms a common starting point to develop high performance catalysts with robust activity for all three CO_2 utilisation reactions. This flexibility in operation would then enable switchable process designs, that adjust to the changing demands in natural gas and chemicals production from CO_2. Processes using switchable catalysts can operate in "Power-to-gas" mode to store renewable energy at times of excess production and can otherwise be switched to the chemicals production mode to supply CO or syngas as carbon building blocks to the chemical industry. Hence, switchable catalysts offer us means to reconcile a continuous supply of captured CO_2 with a variable demand for products of CO_2 utilisation in power-to-gas schemes.

No research has been done into combining these three reactions: DRM, RWGS, and CO_2 methanation. In this study, we show that a single catalyst can be used for all three of them and would enable flexibility needed for a combined power, gas, chemicals and liquid fuels grid, based on the recycling of greenhouse gases. This switchable catalyst should be both active and stable for all of them by altering its temperature and reactants. Our team demonstrated that a combination of 15 wt% Ni and 1 wt% Ru displayed promising activity for the RWGS and CO_2 methanation reactions, resulting in an exceptional performance for CO_2 hydrogenation [31]. The RWGS and CO_2 methanation reactions compete against each other, but due to their different thermodynamic natures, the RWGS reaction is favoured at high temperatures and CO_2 methanation at lower ones. Nevertheless, careful catalyst design is required in the temperature range where the two reactions overlap in order to achieve the desired product selectivity [65,66]. Ni catalysts, promoted with noble metals like Ru have also been used previously for DRM, [18,56] prompting us to explore Ni-Ru bimetallic catalysts as switchable catalysts that can operate with renewable hydrogen or in its absence to recycle greenhouse gases. Consequently, a bimetallic Ni-Ru mixture was chosen to be the active site of the catalysts along with two supports. The first one was CeO_2-Al_2O_3 and the second one $Ce_{0.5}Zr_{0.5}O_2$, which are both promising supports.

2. Experimental

2.1. Catalyst synthesis

The two catalysts were prepared by co-impregnation. Firstly, Ni $(NO_3)_2{\cdot}6H_2O$ (Acros Organics) and $Ru(NO)(NO_3)_3$ solution (1.5 w/v Ru, Alfa Aesar) were mixed in 40 mL of deionised water and added to $Ce_{0.5}Zr_{0.5}O_2$ (Daiichi Kigenso Kagaku Kogyo Co.) in order to obtain a 15 wt% of Ni and 1 wt% of Ru catalyst. The same procedure was followed for the second catalyst, but the support used was a commercial CeO_2-Al_2O_3 support (SCFa-160 Ce20 Puralox, Sasol), containing 20 wt% of CeO_2 and 80 wt% of Al_2O_3.

The two resulting suspensions were initially stirred at room temperature and then concentrated in a rotary evaporator under reduced pressure. After that, the materials obtained were dried at 110 °C overnight and calcined at 500 °C (5 °C/min ramp) for 3 h. For the sake of simplicity, the two catalysts will be referred to as NiRu/CeZr and NiRu/CeAl and the supports as CeZr and CeAl.

2.2. Catalyst characterisation

The specific surface area and the pore volume of each catalyst were calculated by using the Brunauer-Emmett-Teller (BET) equation and the Barett–Joyner–Halenda (BJH) method, respectively. The samples were initially degassed at 250 °C in vacuum for 4 h. Then, nitrogen adsorption–desorption measurements were carried out at liquid nitrogen temperature (-195 °C) in a Micrometrics 3Flex apparatus in order to obtain the textural properties of each catalyst and their supports.

The apparatus used for the X-ray diffraction (XRD) analysis was the X'Pert Powder from PANalytical. The $2\theta^{o}$ angle recorded was over the range of 10-90° with a step size of 0.05° every 240 secs. Additionally, by using a Cu Kα radiation ($\lambda = 0.154$ nm), the diffraction patterns were obtained at 30 mA and 40 kV. XRD analysis was carried out on fresh, reduced at 850 °C for 1 h, post-temperature screening and post-stability experiment samples. The average crystallite size was estimated using the Scherrer equation.

The H_2-Temperature Programmed Reduction (TPR) was conducted

in a continuous fixed bed quartz reactor. A mass spectrometer (Omni-Star GSD 320) measured the H_2 consumption while the data was logged by using the Quadera software package. 50 mg of each catalyst were initially dried at 150 °C with argon (Ar) for 30 mins. After they had cooled down, a flow of 50 mL/min of a 10% H_2/Ar mixture was used while the temperature was increased to 1000 °C with a 10 °C/min rate.

The temperature programmed oxidation (TPO) was carried out on the spent catalyst in the same equipment as H_2-TPR and the data were obtained accordingly. The samples were heated up from room temperature to 900 °C with a 50 mL/min flow of 3% O_2/Ar and a ramp rate of 10 °C/min.

Thermogravimetric analysis (TGA) was conducted on the spent catalyst after the stability test in an SDT Q600 V8.3 Instrument from TA Instruments. A flow of 100 mL/min of air was used, while the temperature was increased from room temperature to 900 °C at 10 °C/min.

X-ray photoelectron spectroscopy (XPS) measurements were carried out in a VGMicrotechMultilab 3000 spectrometer. The XPS spectra were obtained with a hemispherical electron analyser and a Mg Kα (h = 1253.6 eV; 1 eV = 1.6302 × 10–19 J) 300-W X-ray source with a major axis length of 400 μm. The pass energy used was 50 eV. The samples were maintained in the analysis chamber until a residual pressure of ca. 5×10^{-7}N/m^2 was achieved. CasaXPS software was used to carry out the XPS data analysis and the experimental data were fitted in a combination of Lorentzian (30%) and Gaussian (70%) lines. The C1s, whose binding energy (BE) peak was located at 284.6 eV, was used as a reference binding energy. Before the experiment, the samples were reduced *ex situ* at 850 °C and conserved in octane.

2.3. Catalytic activity

All the reactions were carried out in a tubular fixed bed quartz reactor with an outside diameter of 0.5 in, which was placed vertically in a tubular furnace. The catalysts were located on top of a quartz wool bed inside that reactor. A thermocouple was used to enable the monitoring of the temperature throughout the experiments and the deviation from the temperature setpoints if it had occured. An ABB AO2020 online gas analyser was used to detect the amount, i.e. the percentage, of CO_2, CH_4, CO, and H_2 in the product stream after water was separated in a chiller. The initial composition of the reactants was identified using the gas analyser and the total volumetric flow rate was measured using a bubble meter. The bubble meter was used because of the difference in the inlet and exit flow rates. The total outlet flow rate and the composition of the reactants were monitored frequently; they were measured/detected at every temperature in the temperature screening experiments and usually every 30 mins in the stability experiments. In the stability experiment, the trend of the flow rate was found based on the regular measurements, thus enabling the accurate calculation of the various parameters.

Prior to all experiments, an *in situ* reduction was carried out at 850 °C with a 50 mL/min flow of a 10% H_2/N_2 mixture for 1 h. This reduction temperature was selected because of it being the highest operating temperature in our work. The catalysts powder particles used in this project were 100–200 μm. The mass of the catalyst in each temperature screening (TS) experiment was 0.125 g and the weight hourly space velocity (WHSV) 24 L/g h. Two TS experiments were carried out for each catalyst: one for the DRM reaction and one for the RWGS and CO_2 methanation reactions. The inlet stream in the DRM TS experiment had a mole composition of 20% CO_2, 20% CH_4, and 60% N_2, whereas the one in RWGS and CO_2 methanation reactions had a composition of 10% CO_2, 40% H_2, and 50% N_2. All the TS experiments started at the highest temperature and performed by decreasing the temperature in 50 °C increments of 30 mins. The DRM reaction was performed in the 550–850 °C temperature range while the RWGS-CO_2 methanation was conducted across the 200–850 °C range.

In the stability experiment conducted, the reaction temperature was initially 350 °C (CO_2 methanation), increased to 700 °C (RWGS) and finally the reactants were changed at the same temperature, allowing DRM to take place. It was reported in our previous work that the conversion of the NiRu/CeZr catalyst is slightly affected when the stability experiments start with the RWGS instead of the CO_2 methanation reaction [31]. Therefore, the stability experiment in this research started with the CO_2 methanation reaction at 350 °C. The 700 °C temperature was selected so as to observe the deactivation of the catalyst, if any, without having a CO_2 conversion close to 100%. The total flow was 200 mL/min with 10% CO_2, 40% H_2, and 50% N_2 for the RWGS and CO_2 methanation, and 25% CO_2, 25% CH_4, and 50% N_2 for the DRM. The test was performed using 0.1 g of catalyst reaching a WHSV of 120 L/g h. Each reaction was carried out for 20 h, yielding a total time on stream of 60 h.

The equations used for measuring the catalytic activity are presented below (8–14). The F indicates the flow rates of the respective gas and the subscripts in and out refer to the inlet and outlet streams.

$$CO_2\ conversion(\%) = \frac{F_{CO_2,in} - F_{CO_2,out}}{F_{CO_2,in}} \times 100 \quad (8)$$

$$CH_4\ conversion(\%) = \frac{F_{CH_4,in} - F_{CH_4,out}}{F_{CH_4,in}} \times 100 \quad (9)$$

$$CH_4\ selectivity(\%) = \frac{F_{CH_4,out}}{F_{CO_2,in} - F_{CO_2,out}} \times 100 \quad (10)$$

$$CO\ selectivity(\%) = \frac{F_{CO,out}}{F_{CO_2,in} - F_{CO_2,out}} \times 100 \quad (11)$$

$$CO\ yield(\%) = \frac{F_{CO,out}}{F_{CO_2,in}} \times 100 \quad (12)$$

$$CH_4\ yield(\%) = \frac{F_{CH_4,out}}{F_{CO_2,in}} \times 100 \quad (13)$$

$$H_2\ yield(\%) = \frac{F_{H_2,out}}{2 \times F_{CH_4,in}} \times 100 \quad (14)$$

2.4. Thermodynamic simulations

Chemstations' ChemCad software was used so as to acquire the thermodynamic equilibrium conversions for all the reactants of the three reactions over a range of temperatures. The equation of state used was the Soave−Redlich−Kwong. The reactor was simulated as a Gibbs reactor in order to calculate thermodynamic equilibrium limits. The total inlet flow rate and the percentages of the reactants used in the ChemCad simulation were the same as those of both the temperature screening and the stability experiments.

3. Results and discussion

3.1. Textural properties

The textural properties of the catalysts are presented in Table 1. The NiRu/CeAl catalyst had a higher surface area than the NiRu/CeZr, which was expected as alumina is widely used as support due to its large surface area [18,67]. The isotherms of all the catalysts and supports are presented in Figure S1. The type of isotherms generated were Type IV with a characteristic H1 hysteresis loop, according to the IUPAC classification. This suggests the existence of well-developed cylindrical

Table 1
Textural properties of the two catalysts.

Sample	S_{BET} (m^2/g)	V_{PORE} (cm^3/g)	D_{PORE} (nm)
NiRu/CeAl	141	0.29	8.2
NiRu/CeZr	60	0.18	12.6

mesopores [68]. This can be confirmed from the average pore diameter in Table 1.

3.2. Crystalline structure

The XRD patterns for the fresh and reduced NiRu/CeZr and NiRu/CeAl samples are shown in Fig. 1a and Fig. 1b respectively. Both samples presented the characteristic peaks of γ-Al_2O_3 and $Ce_{0.5}Zr_{0.5}O_2$ phases respectively (JCPDS 00–004-0880 & JCPDS 00–038-1436). While CeO_2 was detected in the fresh NiRu/CeAl sample (JCPDS 03–065-5923), it was not detected in the reduced sample. The cerium aluminate phase ($CeAlO_3$) phase was not detected here however its presence was confirmed by XPS. According to previous data found in literature, the $CeAlO_3$ phase should exist in the reduced and in the post-stability samples, but as highly dispersed or incorporated into, or over the other materials [19]. The $CeAlO_3$ phase was in fact detected in the XRD pattern of the sample after H_2-TPR (Figure S2) confirming the restructuration of ceria and alumina. NiO was detected in the fresh samples as there were diffraction peaks at $2\theta^o$ = 37.2°, 43.3°, 62.9° and 75.4° (JCPDS 00–047-1049). Nickel oxide was reduced to metallic Ni^0 in the reduced samples, which was considered as the active species of the reactions (JCPDS 01–070-1849). However, the existence of NiO in the reduced NiRu/CeZr sample suggested that the sample was not fully reduced after the *in situ* reduction (carried out at 850 °C for 1 h). This might have been because of the large nickel particle size maybe in conjunction with mass transfer limitation issues, thus hindering the reduction of internal nickel oxide [67]. $NiAl_2O_4$ spinels were not present in any of the samples. As for Ru crystalline phases, traces of RuO_2 appeared in the fresh samples (JCPDS 01–070-2662) and of metallic Ru^0, in the reduced NiRu/CeAl sample (JCPDS 01–070-0274). The estimate metallic Ni particle size using the Scherrer equation at $2\theta^o$ = 44.48° were 12.4 and 34.1 nm for the NiRu/CeAl and NiRu/CeZr respectively.

3.3. Reducibility: H_2 – TPR

The redox properties and the interactions between the support and the metallic species are observed in the H_2 temperature programmed reduction. The H_2-TPR profiles of the CeAl, CeZr, NiRu/CeAl, and the NiRu/CeZr are shown in Fig. 2. Overall, it was observed that Ni and Ru shifted the reduction of the supports at lower temperatures pointing out an intimate metal-support interaction.

As regards the CeAl support, a wide reduction process was observed. Ceria surface reduction took place between 150 °C and 700 °C, while the peak at 850 °C was attributed to the reduction of the bulk ceria

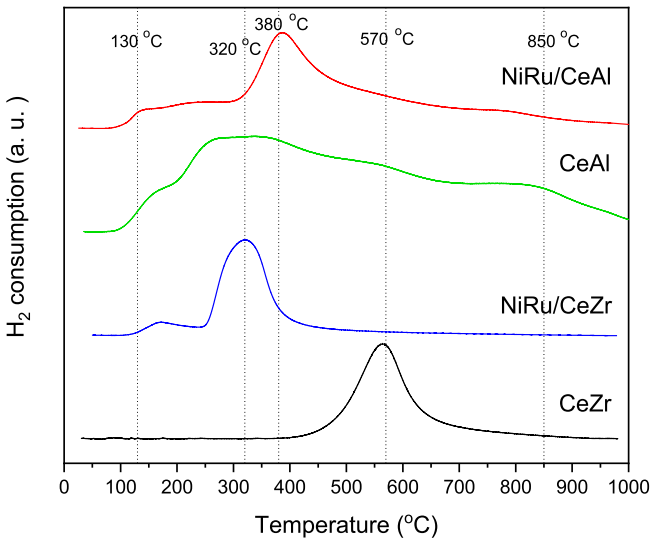

Fig. 2. H_2-TPR profiles for NiRu/CeAl, CeAl, NiRu/CeZr, CeZr.

crystallites. When Ni and Ru were added, the reduction of ceria was facilitated, showing a close Ni-CeO_2 interaction [38,69]. The peak at 380 °C was mainly attributed to the reduction of the medium-sized NiO_x species interacting with the CeO_2 particles [31,69,70]. In the CeZr sample, a peak at 570 °C was evident where the reduction of Ce^{4+} to Ce^{3+} occurred. Concerning the NiRu/CeZr, the main peak at 320 °C was due to the surface oxygen reduction of CeZr and the Ni^{2+} species interacting with the support. It appeared that Ni-Ru facilitated the reduction of the surface oxygen of the CeZr support, thus shifting the main reduction peak towards lower temperatures, showing the interaction between the Ni and Ru species and the support. In the NiRu/CeAl and NiRu/CeZr samples, the peaks at 130 °C and 170 °C respectively corresponded to the reduction of Ru^{4+} to metallic Ru and their difference in the reduction peak position was associated with different forms of interaction with the support [31,55]. In general, a strong interaction of the Ni species with the support is associated with a high catalytic activity [71,72]. We will discuss this potential correlation within the studied CO_2 conversion reactions in the next sections.

3.4. Surface composition of catalysts

XPS was performed on reduced catalysts to obtain information about the chemical state of the elements and coordination environments of Ni

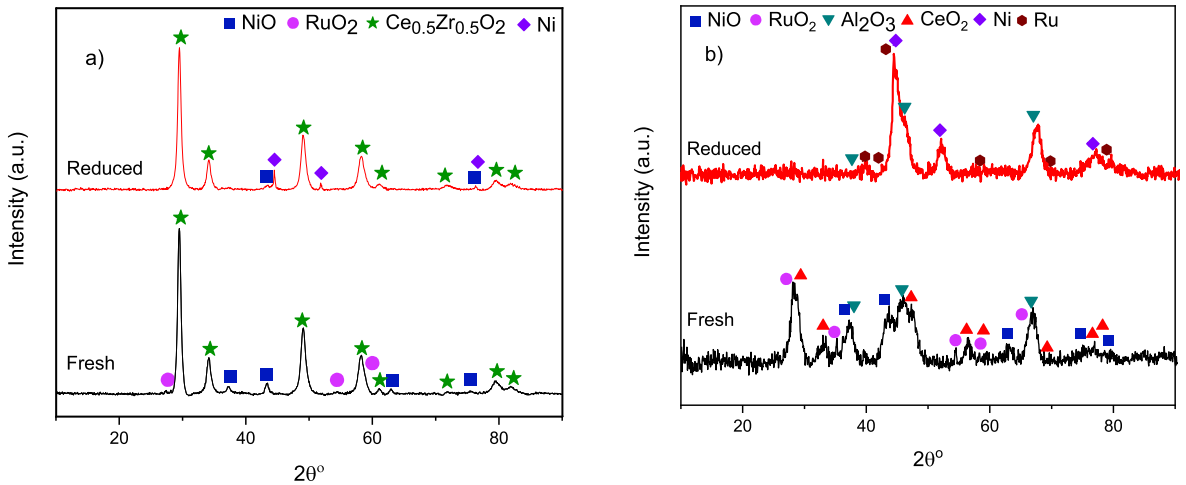

Fig. 1. XRD patterns of the fresh and reduced catalysts: a) NiRu/CeZr and b) NiRu/CeAl.

and Ru surface species.

Figure 3a shows the Ni2p$_{3/2}$ spectra of the two reduced catalysts. In both catalysts, a mixture of metallic Ni (851–853 eV) and Ni^{2+} (854–857 eV) was observed [31]. Therefore, the Ni^{2+} species were not fully reduced upon the reduction treatment employed prior to reaction for any of the catalysts. However, there was a higher amount of metallic nickel in the NiRu/CeZr sample compared to that of the NiRu/CeAl, as reported in the Ni^0/Ni_{Total} ratio in Table 2. This indicated that there was a strong metal-support interaction that facilitated the reduction of nickel oxide to metallic nickel in that sample. Regarding the NiRu/CeAl catalyst, it appeared that there was a higher amount of oxidised nickel, which was also evident in the H_2-TPR results (Fig. 2), showing a slow rate of reduction after 450 °C. Moreover, the Ni/support ratio observed in Table 2 was higher in the NiRu/CeZr sample, indicating that a significantly higher Ni dispersion at the surface was achieved. In contrast with the XRD results, which suggested that only the Ni in the NiRu/CeZr hadn't been fully reduced, the XPS results illustrated that there was a higher amount of NiO in the NiRu/CeAl sample. The latter suggest a slightly different surface (XPS) and bulk (XRD) compositions which is common in this kind of Ni-based systems [31].

The binding energies of Ru3p$_{3/2}$ are presented in Table 2 and its spectra in Fig. 3b. Similarly to nickel, both metallic Ru and Ru^{4+} existed in the two samples. However, the ratio of Ru^0/Ru_{Total} indicated that there was a higher amount of metallic Ru in the NiRu/CeAl sample, showing a higher reducibility of the Ru species in good agreement with the H_2-TPR results. Additionally, a higher value was obtained for the Ru/support ratio in the case of NiRu/CeZr. This suggests that a higher Ru dispersion at the surface was achieved in that sample, which was in good agreement with its XRD data and with the absence of Ru^0 in its reduced form.

The Ce3d region is presented in Fig. 3c. A mixture of Ce^{3+} and Ce^{4+} was present in the NiRu/CeAl sample, corresponding to $CeAlO_3$ and CeO_2, respectively. This was particularly evident in the significantly diminished peak at ~ 917 eV, suggesting a considerably lower amount of Ce^{4+} [19,73]. The $CeAlO_3$ phase was also detected by XRD on this catalyst after H_2-TPR (Figure S2). A mixture of Ce^{3+} and Ce^{4+} was also observed in the NiRu/CeZr sample, thus both Ce_2O_3 and CeO_2 existed.

3.5. Catalytic behaviour

3.5.1. Temperature screening experiments

The catalysts' performance as regards the CO_2 conversion in DRM is presented in Fig. 4a, while the H_2/CO ratio in Fig. 4b. It can be seen that the two catalysts exhibited very similar performance. At higher temperatures, i.e. above 750 °C, the CO_2 conversions reached thermodynamic equilibrium. As the DRM is an endothermic reaction, higher temperatures are needed in order to achieve higher conversions. At lower temperatures, the NiRu/CeAl catalyst performed slightly better than the NiRu/CeZr. Nevertheless, the two catalysts appeared to have very similar CO_2 conversion.

As far as the CH_4 conversion was concerned, which can be seen in Figure S3, both catalysts were below the equilibrium, even at high temperatures. The NiRu/CeAl sample performed better overall, with a difference in CH_4 conversion between the catalysts being as high as 13% at 700°C, i. e. 62% for the NiRu/CeAl and 49% for the NiRu/CeZr. In general, CH_4 conversion is smaller than that of CO_2 due to two phenomena. Firstly, the energy barrier of methane activation, which is considered to be the rate-determining step, is larger than that of carbon dioxide activation. Secondly, the presence of carbon dioxide and hydrogen drives the RWGS, which is a side reaction of the DRM.

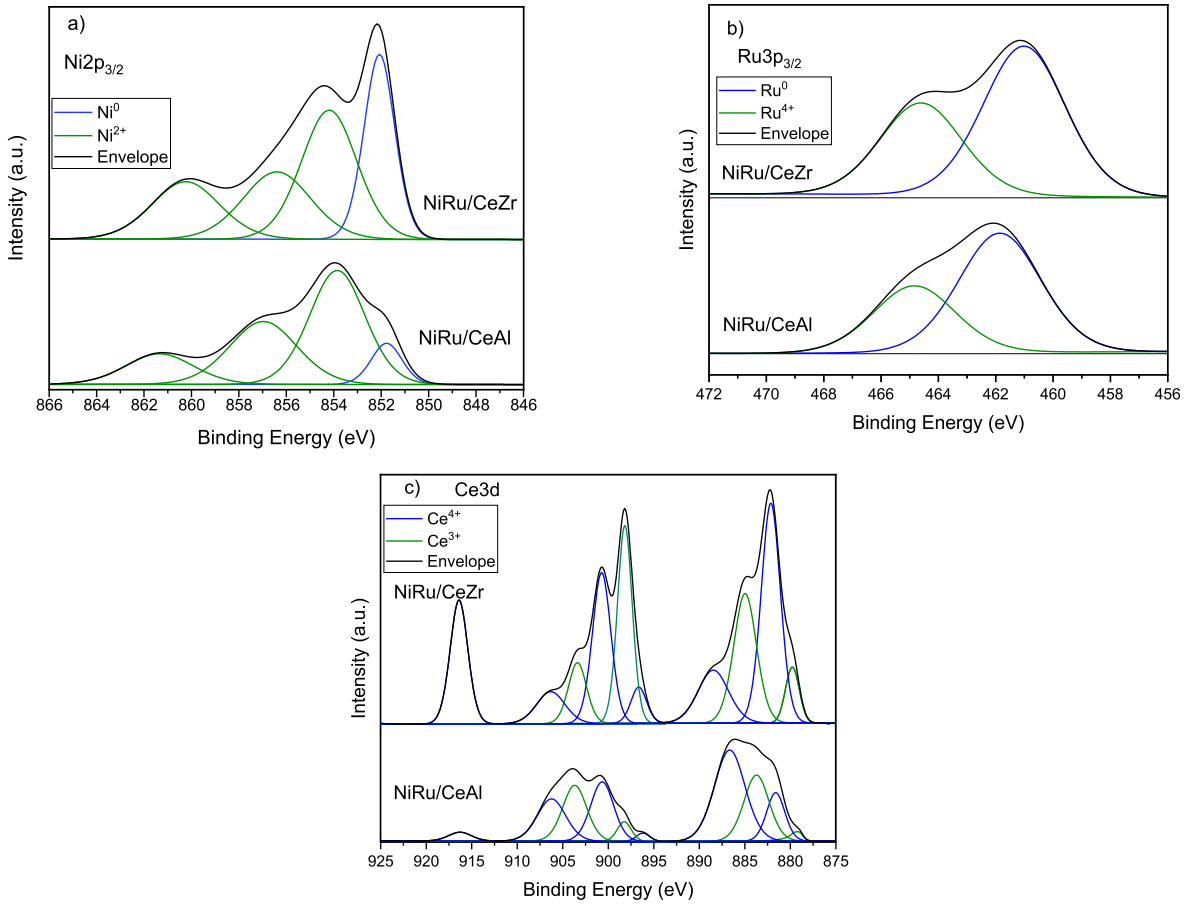

Fig. 3. XPS spectra of the a) Ni 2p3/2, b) Ru 3p3/2 and c) Ce 3d regions for the two catalysts.

Table 2
Binding Energies of the Ni 2p3/2 and Ru 3p3/2 levels for the reduced catalysts and Ni/support, Ni^0/Ni_{Total} and Ru^0/Ru_{Total} atomic ratios.

Catalyst	Ni $2p_{3/2}$ (eV)		Ru $3p_{3/2}$ (eV)		Ni/(Ce + Zr or Al)	Ni^0/Ni_{Total}	Ru/(Ce + Zr or Al)	Ru^0/Ru_{Total}
	Ni^0	Ni^{2+}	Ru^0	Ru^{4+}				
NiRu/CeZr	852.1	854.2–856.4	461.0	464.6	0.096	0.267	0.035	0.621
NiRu/CeAl	851.8	853.9–856.9	461.9	464.9	0.040	0.091	0.017	0.642

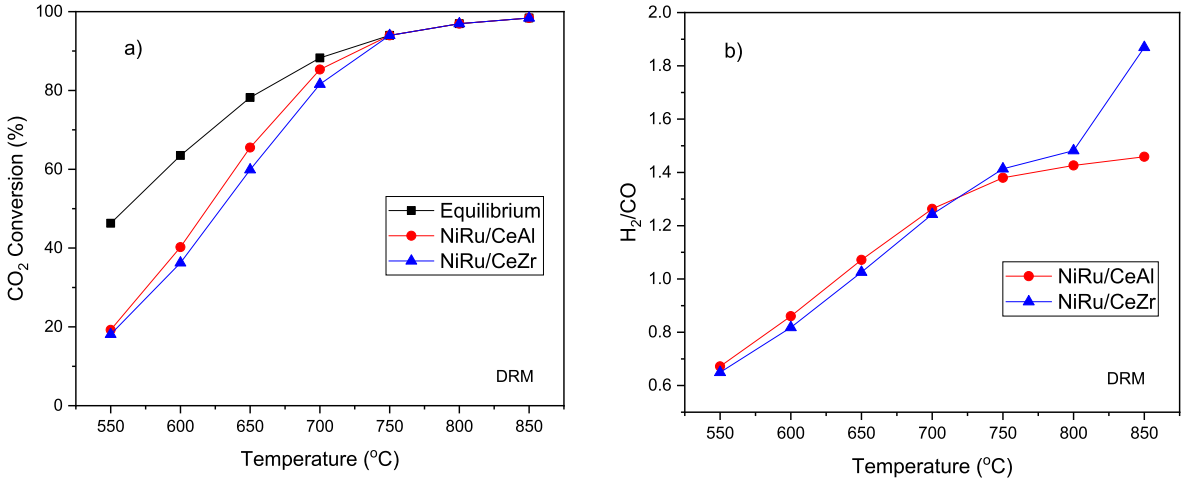

Fig. 4. DRM temperature screening experiment for NiRu/CeAl, NiRu/CeZr and at equilibrium: a) CO_2 conversion and b) H_2/CO ratio ($CO_2/CH_4/N_2$: 1/1/3, P = 1 atm, WHSV = 24 $L.g^{-1}.h^{-1}$).

Therefore, an amount of CO_2 reacts with H_2 instead of CH_4 and it is eventually converted into CO [34,74].

Just as in the CO_2 conversion, the H_2/CO ratio did not vary significantly for the two catalysts. As aforementioned, this ratio should be 1 for the DRM. However, it was evident that above 650 °C, this ratio was above 1 as a result of two events. Firstly, since the RWGS is a side reaction of the DRM, H_2O is present in the reactor. Therefore, the bi-reforming reaction, which has a syngas ratio of 2, occurs simultaneously [38,75]. Secondly, methane decomposition (7) also takes place. Consequently, an excess amount of H_2 is produced, increasing the ratio [34]. The methane decomposition was evident in the NiRu/CeZr sample at 850 °C. This increased value in Fig. 4b is in agreement with the CH_4 conversion of that catalyst at the same temperature (Figure S3). Additionally, the H_2/CO ratio was below 1 for temperatures under 650 °C due to the RWGS [34].

Although the two catalysts showed similar performance in DRM, different behaviours were obtained for CO_2 hydrogenation. The CO_2 conversion and the CO and CH_4 selectivity of the two catalysts in the RWGS and CO_2 methanation reactions are presented in Fig. 5a and Fig. 5b, respectively. The CO_2 conversion for both catalysts reached the equilibrium values at higher temperatures. It might have been due to the fact that CeO_2 also catalyses the RWGS, due to the existence of nearby oxygen vacancies at the nickel-ceria interface being considered as efficient active site for CO_2 hydrogenation [58]. Concerning the methanation reaction, it was clear that the NiRu/CeAl catalyst had a superior activity; it achieved equilibrium conversion at a temperature as low as 350 °C. As this is reaction is structure sensitive [53,76], it was suggested that their difference in the CO_2 conversion was due to the smaller particle size of Ni in the NiRu/CeAl catalyst in good agreement with our XRD data. In addition to that, it is known that the CO_2 conversion is improved when the Ce^{3+} is stabilised in the form of $CeAlO_3$, which acts as a driving force for CO_2 activation [77], thus further boosting the

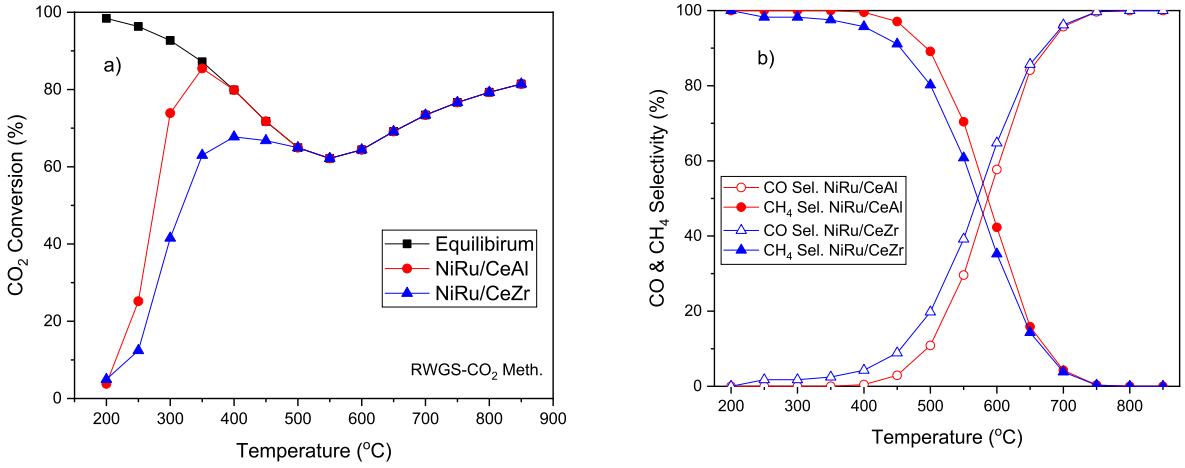

Fig. 5. RWGS-CO_2 methanation temperature screening experiment for NiRu/CeAl, NiRu/CeZr and at equilibrium: a) CO_2 conversion and b) CO and CH_4 selectivity ($CO_2/H_2/N_2$: 1/4/5, P = 1 atm, WHSV = 24 $L.g^{-1}.h^{-1}$).

activity of this catalyst.

The CO selectivity is increased with increasing temperature, while the opposite is true for the CH_4 selectivity. More specifically, RWGS was favoured at temperatures higher than 550–600 °C, and CO_2 methanation at lower ones. Fig. 5b shows that above 750 °C, both catalysts showed 100% CO selectivity due to the endothermic nature of RWGS. Below 700 °C, the NiRu/CeZr showed a higher selectivity towards CO, and the NiRu/CeAl towards CH_4. At 400 °C, the latter achieved a 100% CH_4 selectivity, demonstrating its excellent performance. The NiRu/CeZr catalyst reached 100% CH_4 selectivity at 200 °C, but at such low temperatures, CO_2 conversion was less than 5%. The difference in selectivity of the two catalysts was attributed to smaller particle size of the NiRu/CeAl catalysts, which favoured the CH_4 formation instead of CO [76] and to the $CeAlO_3$ phase, which enhanced the CO_2 activation in the CO_2 methanation reaction.

Certainly, the CO_2 activation offered us a starting point in order to search for switchable catalysts. The results of the catalytic activity experiments showed that the Ni-Ru catalysts are active for the dry reforming of methane, the reverse water–gas shift and the CO_2 methanation. Especially NiRu/CeAl is a very active catalyst for all the CO_2 utilisation reactions, which can provide us with the opportunity to provide chemicals and fuel in various power-to-gas schemes.

3.5.2. Stability experiment

The stability experiments are an essential part of catalytic research as they showcase whether the catalyst is durable and how much it is affected by coking and/or sintering over time. Additionally, as our vision of switchable catalysts is not only to be active in all the CO_2 utilisation reaction, but also to be stable in all of them. The switchable catalyst should be stable in these reactions while the modes are switched from the "Power-to-gas" mode" to store renewable energy at times of excess production to the chemicals-production mode to supply CO or syngas as carbon building blocks to the chemical industry and vice versa. As NiRu/CeAl showed overall a better activity compared to NiRu/CeZr, it was selected for the stability experiments.

In the stability experiment, the NiRu/CeAl catalyst manifested an impressive performance and stability in the CO_2 methanation; the CO_2 conversion remained constant at 70% after 20 h, while the methane yield was 69% throughout the entire duration. The NiRu/CeAl was also very stable in the RWGS reaction, having a 73% conversion, which is that of the equilibrium, and a 56% CO yield. These results indicated the excellent stability of the bi-metallic Ni-Ru catalysts in the CO_2 hydrogenation reactions in line with our previous findings [31]. It should be noted that the methanation performance of NiRu/CeAl was different in the stability experiment compared to the temperature screening experiment because of the higher space velocity used in the former. As far as the stability of the catalyst in the DRM was concerned, Fig. 6 shows that the catalyst maintained a CO_2 conversion of 71% after 10 h on stream. After 20 h on stream, that conversion decreased by 10% mainly due to the catalyst's coke formation as shown by post reaction characterisation (Section 3.6). It is worth noting that the space velocity used was higher than the 10,000 h^{-1} operational space velocities for static reformers in industrial applications [38,78]. In any case, the excellent behaviour of our switchable catalyst under very high space velocity is commendable. Beyond the product flexibility, its performance at a high space velocity involves a significant reduction of the overall reactor volume (and hence its capital costs) thus allowing the design of compact CO_2 conversion units.

Undoubtedly, the impressive stability of NiRu/CeAl makes it an ideal candidate catalyst for our vision to use switchable catalysts in the various CO_2 utilisation scenarios. This catalyst showed a stable CO_2 conversion, even when the conditions changed, which is an important characteristic that a switchable catalyst should have. Obviously, NiRu/CeAl catalyst has manifested a remarkable stability performance in the CO_2 hydrogenation reactions, but a catalyst improvement is needed to further enhance its performance in the DRM reaction and accomplish a stable cyclic operation between these three CO_2 utilisation reactions.

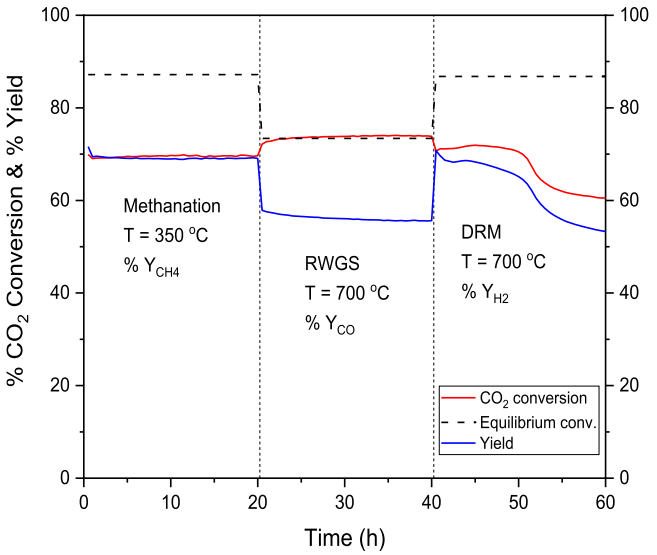

Fig. 6. NiRu/CeAl stability test: CO_2 conversions and product for CO_2 methanation ($CO_2/H_2/N_2$: 1/4/5, T = 350 °C), RWGS ($CO_2/H_2/N_2$: 1/4/5, T = 700 °C) and DRM ($CO_2/CH_4/N_2$: 1/1/2, T = 700 °C) at WHSV = 120 $L.g^{-1}.h^{-1}$.

4. Post characterisation

4.1. 1 X-Ray diffraction (XRD)

The XRD patterns for the post temperature screening NiRu/CeZr and NiRu/CeAl samples are shown in Fig. 7a and Fig. 7b respectively. In the NiRu/CeZr XRD pattern, there was no NiO in contrast with the reduced sample (Fig. 1a) meaning that the remaining NiO was converted into metallic Ni during the reaction. A closer observation shows that there was a small carbon peak after the DRM temperature screening experiment (TS), suggesting that the catalyst had started to deactivate. This is in line with the methane decomposition observed during the TS experiment. However, there was no crystalline carbon peak in the NiRu/CeAl sample. By applying the Scherrer equation to find the average particle size of Ni, the extent of sintering was observed. The average Ni particle size was estimated to be 12.5 nm both post RWGS-CO_2 methanation and DRM TS for NiRu/CeAl and 33.5 nm post RWGS-CO_2 methanation TS and 34.7 nm post DRM TS for NiRu/CeZr (compared to the initial 12.4 and 34.1 nm for the NiRu/CeAl and NiRu/CeZr respectively). The minor differences on Ni particle size found in the reduced NiRu/CeZr sample was considered to be within the error limits during the calculations. Negligible sintering was observed in the NiRu/CeAl samples after the TS experiments. Concerning NiRu/CeZr, it was observed that sintering affected that catalyst more during DRM than RWGS and CO_2 methanation, suggesting that sintering is dependent on the reaction mixture. This might have been because of the formation of coke, which is generally known to enhance sintering, and/or the slow sintering rate in a H_2 atmosphere, thus in the CO_2 hydrogenation reactions [79].

The XRD pattern of the spent catalysts after the stability experiment are shown in Fig. 8. A carbon peak was observed at $2\theta^o = 26°$, indicating the crystalline coke formation following the stability experiment. Additionally, Fig. 8 reveals the extent of the sintering phenomenon, which resulted in a slight catalyst deactivation during DRM, as Ni particle size was calculated to be 14.3 nm. Consequently, there was a small degree of metallic sintering. In general, an increase in the Ni particle size was expected because the reactions temperatures of the RWGS and DRM were higher than the Tammann temperature of Ni [64]. Therefore, the catalyst deactivation observed in the DRM stability was attributed to a slight degree of sintering, but mainly to carbon deposition.

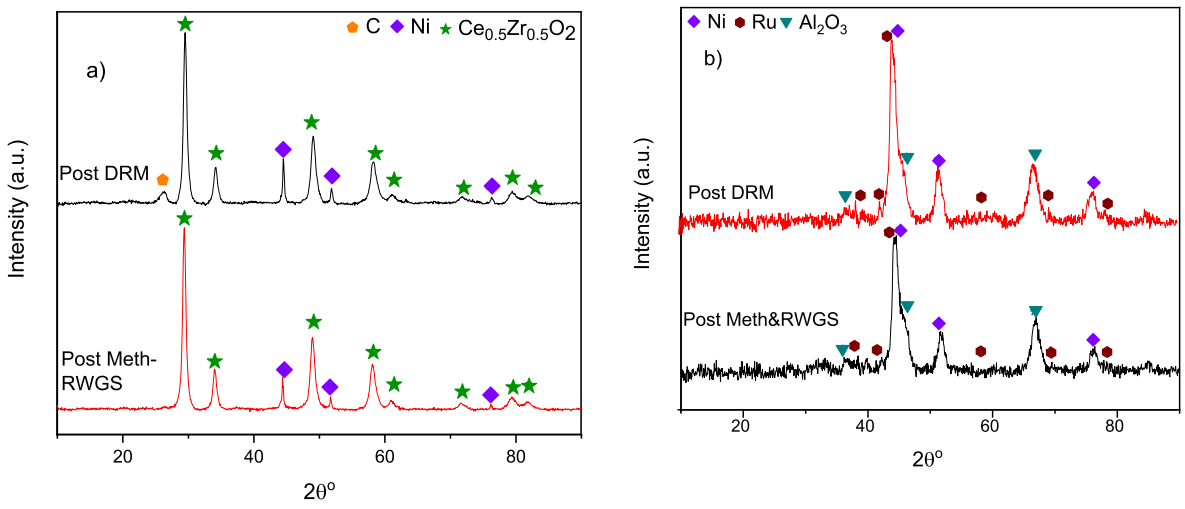

Fig. 7. XRD patterns of the catalysts after the temperature screening experiments: a) NiRu/CeZr and b) NiRu/CeAl.

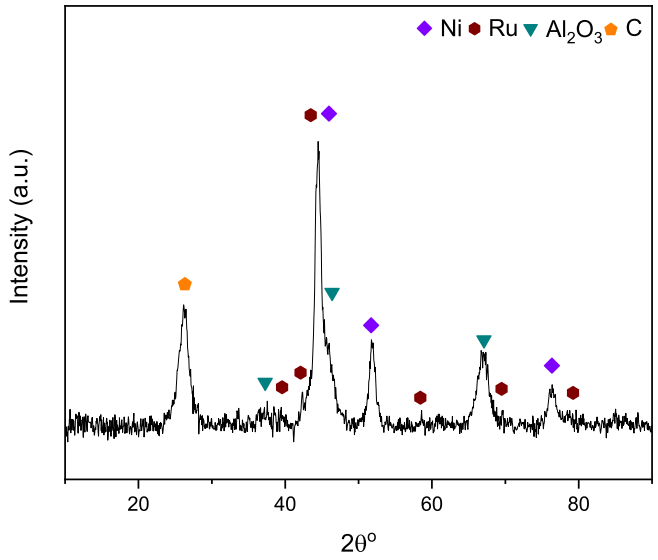

Fig. 8. XRD pattern for the NiRu/CeAl catalyst after the stability experiment.

4.1.1. *Carbonaceous deposits*

As indicated in the XRD, crystalline carbonaceous deposits were detected on the samples. Fig. 9a shows the thermogravimetric analysis (TGA) performed on the post stability sample, while Fig. 9b shows its TPO profile.

The TGA plot shows the amount of coke deposition formed after 60 h on stream. It was observed that there was a carbon formation of 0.29 g_c/g_{cat} in the spent sample. The TPO profile shows two distinct peaks, meaning that multiple carbon types were present in the sample. The peaks at lower temperatures indicated the existence of softer carbon with a poorer degree of crystallinity, while the peaks at higher temperatures indicated the existence of harder carbon with greater degree of crystallinity. Harder carbon requires higher temperature to oxidise, while softer carbon can be regenerated at mild conditions [38]. Therefore, the formation of softer carbon is more desirable compared to harder. Hence, in the TPO profile it was observed that there was a bigger amount of softer carbon, which is more advantageous if regeneration is to be performed. Overall, there was a high amount of carbon being formed indicated that further improvement of the catalyst is needed in the future. In any case, as positive outcome of the carbon deposits study, our TPO data indicate that no matter the reaction conditions the carbon deposits can be burned at relatively mild temperatures (700 °C) opening excellent opportunities for catalysts regeneration.

5. Conclusions

We report for the first time a switchable Ni-Ru catalyst able to effectively catalyse three CO_2 utilisation reactions in the gas phase, i.e. dry reforming of methane, reverse water–gas shift, and carbon dioxide

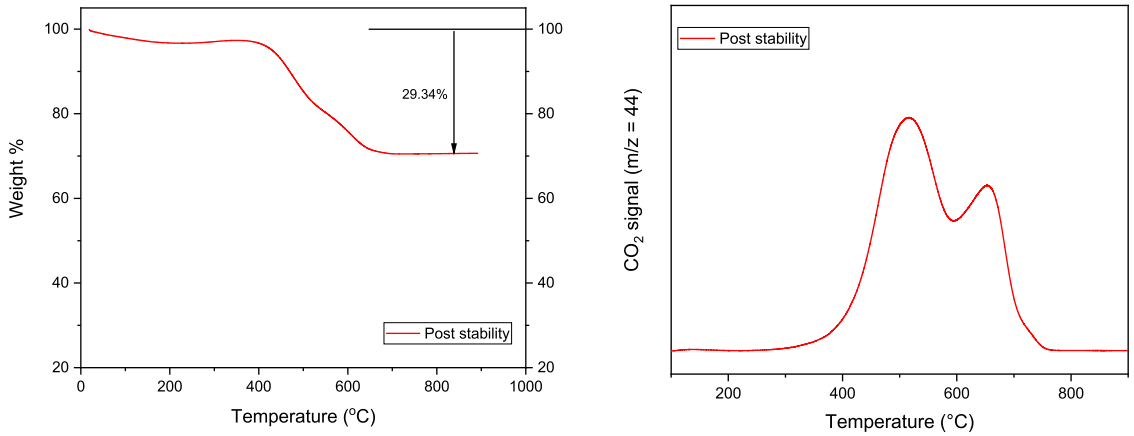

Fig. 9. (a) Thermogravimetric analysis and (b) TPO of the spent NiRu/CeAl catalyst after the stability test.

methanation. Such switchable catalyst allows flexibility in synthesis of chemicals from CO_2.

This study specifically examined the impact of the supports on the performance of a Ni-Ru catalyst. The physiochemical properties of the different catalysts were studied while their activities were tested over a range of temperatures and times on stream for all the reactions. The positive effects of a Ce-Al support were observed. The increased specific surface area of the NiRu/CeAl catalyst, attributed to the alumina content, and its Ni small particle size result are advantageous. Indeed, the Ce-Al catalyst showed remarkable activity and stability levels in the CO_2 methanation and RWGS reactions while maintaining a high yield to desired products CH_4 and CO respectively. Especially in the CO_2 methanation reaction, this catalyst was very active, mainly due to its small particle size. Similar successful results were also obtained for the DRM reaction, during which some degree of deactivation occurred. Deactivation due to carbon deposition was observed in the DRM stability experiment and motivates further development of switchable catalysts with increased resistance to coking in order to establish a cyclic operation between these three CO_2 utilisation reactions. Our TPO results encourage a potential catalyst regeneration at temperatures around 700 °C.

Overall, this paper outlines a novel direction for combating CO_2 emissions by developing catalysts for not individual CO_2 utilisation schemes but for a switchable operation scenario allowing for flexibility in CO_2 recycling based on renewable electricity availability and changing product demands. The NiRu/CeAl catalyst offers this opportunity to control products of CO_2 utilisation using reactant composition and temperature, and it is a major step towards our vision of adaptable CO_2 recycling.

CRediT authorship contribution statement

Loukia-Pantzechroula Merkouri: Formal analysis, Investigation, Writing – original draft. **Estelle le Saché:** Investigation, Methodology, Writing – review & editing. **Laura Pastor-Pérez:** Investigation. **Melis S. Duyar:** Supervision, Writing – review & editing. **Tomas Ramirez Reina:** Conceptualization, Funding acquisition, Methodology, Supervision, Writing – review & editing.

Declaration of Competing Interest

The authors declare that they have no known competing financial interests or personal relationships that could have appeared to influence the work reported in this paper.

Acknowledgements

Financial support for this work was provided by the Department of Chemical and Process Engineering and the Doctoral College of the University of Surrey. The work was partially sponsored by the Royal Society Research Grant RSGR1180353 and the CO2ChemUK through the EPSRC grant EP/P026435/1.

Appendix A. Supplementary data

Supplementary data to this article can be found online at https://doi.org/10.1016/j.fuel.2021.123097.

References

[1] Pires JCM, Martins FG, Alvim-Ferraz MCM, Simões M. Recent developments on carbon capture and storage: an overview. Chem Eng Res Des 2011;89:1446–60. https://doi.org/10.1016/j.cherd.2011.01.028.
[2] IEA, Global CO2 emissions in 2020, (2021). https://www.iea.org/articles/global-energy-review-co2-emissions-in-2020 (accessed August 7, 2021).
[3] Yang H, Xu Z, Fan M, Gupta R, Slimane RB, Bland AE, et al. Progress in carbon dioxide separation and capture: a review. J Environ Sci 2008;20:14–27. https://doi.org/10.1016/S1001-0742(08)60002-9.
[4] Dlugokencky TP Ed, Trends in Atmospheric Carbon Dioxide, NOAA. (2021). ftp://aftp.cmdl.noaa.gov/products/trends/co2/co2_mm_gl.txt (accessed July 6, 2021).
[5] Gibbins J, Chalmers H. Carbon capture and storage. Energy Policy. 2008;36:4317–22. https://doi.org/10.1016/j.enpol.2008.09.058.
[6] Wang W, Wang S, Ma X, Gong J. Recent advances in catalytic hydrogenation of carbon dioxide. Chem Soc Rev 2011;40:3703–27. https://doi.org/10.1039/c1cs15008a.
[7] Peters M, Köhler B, Kuckshinrichs W, Leitner W, Markewitz P, Müller TE. Chemical technologies for exploiting and recycling carbon dioxide into the value chain. ChemSusChem 2011;4:1216–40. https://doi.org/10.1002/cssc.201000447.
[8] Al-Mamoori A, Krishnamurthy A, Rownaghi AA, Rezaei F. Carbon capture and utilization update. Energy Technol. 2017;5:834–49. https://doi.org/10.1002/ente.201600747.
[9] Quadrelli EA, Centi G, Duplan JL, Perathoner S. Carbon dioxide recycling: emerging large-scale technologies with industrial potential. ChemSusChem 2011;4:1194–215. https://doi.org/10.1002/cssc.201100473.
[10] le Saché E, Pastor-Pérez L, Garcilaso V, Watson DJ, Centeno MA, Odriozola JA, et al. Flexible syngas production using a La2Zr2-xNixO7-δ pyrochlore-double perovskite catalyst: towards a direct route for gas phase CO2 recycling. Catal Today 2020;357:583–9. https://doi.org/10.1016/j.cattod.2019.05.039.
[11] Olah GA, Goeppert A, Czaun M, Prakash GKS. Bi-reforming of methane from any source with steam and carbon dioxide exclusively to metgas (CO-2H2) for methanol and hydrocarbon synthesis. J Am Chem Soc 2013;135:648–50. https://doi.org/10.1021/ja311796n.
[12] Jahangiri H, Bennett J, Mahjoubi P, Wilson K, Gu S. A review of advanced catalyst development for Fischer-Tropsch synthesis of hydrocarbons from biomass derived syn-gas. Catal Sci Technol 2014;4:2210–29. https://doi.org/10.1039/c4cy00327f.
[13] Le TA, Kim MS, Lee SH, Kim TW, Park ED. CO and CO2 methanation over supported Ni catalysts. Catal Today 2017;293–294:89–96. https://doi.org/10.1016/j.cattod.2016.12.036.
[14] Götz M, Lefebvre J, Mörs F, McDaniel Koch A, Graf F, Bajohr S, et al. Renewable power-to-gas: a technological and economic review. Renew Energy 2016;85:1371–90. https://doi.org/10.1016/j.renene.2015.07.066.
[15] Pastor-Pérez L, Le Saché E, Jones C, Gu S, Arellano-Garcia H, Reina TR. Synthetic natural gas production from CO2 over Ni-x/CeO2-ZrO2 (x = Fe, Co) catalysts: influence of promoters and space velocity. Catal Today 2018;317:108–13. https://doi.org/10.1016/j.cattod.2017.11.035.
[16] Nikoo MK, Amin NAS. Thermodynamic analysis of carbon dioxide reforming of methane in view of solid carbon formation. Fuel Process Technol 2011;92:678–91. https://doi.org/10.1016/j.fuproc.2010.11.027.
[17] Gomes R, Costa D, Junior R, Santos M, Rodella C, Fréty R, et al. Dry reforming of methane over nila-based catalysts: Influence of synthesis method and ba addition on catalytic properties and stability. Catalysts 2019;9. https://doi.org/10.3390/catal9040313.
[18] Pakhare D, Spivey J. A review of dry (CO2) reforming of methane over noble metal catalysts. Chem Soc Rev 2014;43:7813–37. https://doi.org/10.1039/c3cs60395d.
[19] Price CAH, Arnold W, Pastor-Pérez L, Amini-Horri B, Reina TR. Catalytic upgrading of a biogas model mixture via low temperature DRM using multicomponent catalysts. Top Catal 2020;63:281–93. https://doi.org/10.1007/s11244-019-01216-8.
[20] Guharoy U, Le Saché E, Cai Q, Reina TR, Gu S. Understanding the role of Ni-Sn interaction to design highly effective CO2 conversion catalysts for dry reforming of methane. J CO2 Util 2018;27:1–10. https://doi.org/10.1016/j.jcou.2018.06.024.
[21] Wolfbeisser A, Sophiphun O, Bernardi J, Wittayakun J, Föttinger K, Rupprechter G. Methane dry reforming over ceria-zirconia supported Ni catalysts. Catal Today 2016;277:234–45. https://doi.org/10.1016/j.cattod.2016.04.025.
[22] Charisiou ND, Siakavelas G, Papageridis KN, Baklavaridis A, Tzounis L, Avraam DG, et al. Syngas production via the biogas dry reforming reaction over nickel supported on modified with CeO2 and/or La2O3 alumina catalysts. J Nat Gas Sci Eng 2016;31:164–83. https://doi.org/10.1016/j.jngse.2016.02.021.
[23] Nakhaei Pour A, Mousavi M. Combined reforming of methane by carbon dioxide and water: particle size effect of Ni-Mg nanoparticles. Int J Hydrogen Energy 2015;40:12985–92. https://doi.org/10.1016/j.ijhydene.2015.08.011.
[24] Movasati A, Alavi SM, Mazloom G. CO2 reforming of methane over Ni/ZnAl2O4 catalysts: influence of Ce addition on activity and stability. Int J Hydrogen Energy 2017;42:16436–48. https://doi.org/10.1016/j.ijhydene.2017.05.199.
[25] Pastor-Pérez L, Shah M, Le Saché E, Reina TR. Improving Fe/Al 2 O 3 catalysts for the reverse water-gas shift reaction: on the effect of cs as activity/selectivity promoter. Catalysts 2018;8. https://doi.org/10.3390/catal8120608.
[26] Daza YA, Kuhn JN. CO2 conversion by reverse water gas shift catalysis: Comparison of catalysts, mechanisms and their consequences for CO2 conversion to liquid fuels. RSC Adv 2016;6:49675–91. https://doi.org/10.1039/c6ra05414e.
[27] Park SW, Joo OS, Jung KD, Kim H, Han SH. Development of ZnO/Al2O3 catalyst for reverse-water-gas-shift reaction of CAMERE (carbon dioxide hydrogenation to form methanol via a reverse-water-gas-shift reaction) process. Appl. Catal. A Gen. 2001;211:81–90. https://doi.org/10.1016/S0926-860X(00)00840-1.
[28] Park SW, Joo OS, Jung KD, Kim H, Han SH. ZnO/Cr2O3 catalyst for reverse-water-gas-shift reaction of CAMERE process. Korean J Chem Eng 2000;17:719–22. https://doi.org/10.1007/BF02699123.
[29] Joo OS, Jung KD, Moon I, Rozovskii AY, Lin GI, Han SH, et al. Carbon dioxide hydrogenation to form methanol via a reverse-water-gas- shift reaction (the CAMERE process). Ind Eng Chem Res 1999;38:1808–12. https://doi.org/10.1021/ie9806848.

[30] Samimi F, Rahimpour MR, Shariati A. Development of an efficient methanol production process for direct CO2 hydrogenation over a Cu/Zno/Al2O3 catalyst. Catalysts. 2017;7. https://doi.org/10.3390/catal7110332.

[31] Le Saché E, Pastor-Pérez L, Haycock BJ, Villora-Picó JJ, Sepúlveda-Escribano A, Reina TR. Switchable catalysts for chemical CO2 recycling: a step forward in the methanation and reverse water-gas shift reactions. ACS Sustain. Chem. Eng. 2020; 8:4614–22. https://doi.org/10.1021/acssuschemeng.0c00551.

[32] Martínez J, Hernández E, Alfaro S, Medina RL, Aguilar GV, Albiter E, et al. High selectivity and stability of nickel catalysts for CO2 Methanation: Support effects. Catalysts 2019;9. https://doi.org/10.3390/catal9010024.

[33] Koytsoumpa EI, Karellas S, Kakaras E. Modelling of substitute natural gas production via combined gasification and power to fuel. Renew. Energy 2019;135: 1354–70. https://doi.org/10.1016/j.renene.2018.09.064.

[34] le Saché E, Pastor-Pérez L, Watson D, Sepúlveda-Escribano A, Reina TR. Ni stabilised on inorganic complex structures: superior catalysts for chemical CO2 recycling via dry reforming of methane. Appl. Catal. B Environ. 2018;236:458–65. https://doi.org/10.1016/j.apcatb.2018.05.051.

[35] Brooks KP, Hu J, Zhu H, Kee RJ. Methanation of carbon dioxide by hydrogen reduction using the Sabatier process in microchannel reactors. Chem Eng Sci 2007; 62:1161–70. https://doi.org/10.1016/j.ces.2006.11.020.

[36] Duyar MS, Ramachandran A, Wang C, Farrauto RJ. Kinetics of CO2 methanation over Ru/γ-Al2O3 and implications for renewable energy storage applications. J CO2 Util 2015;12:27–33. https://doi.org/10.1016/j.jcou.2015.10.003.

[37] Gao J, Wang Y, Ping Y, Hu D, Xu G, Gu F, et al. A thermodynamic analysis of methanation reactions of carbon oxides for the production of synthetic natural gas. RSC Adv 2012;2:2358–68. https://doi.org/10.1039/c2ra00632d.

[38] Stroud T, Smith TJ, Le Saché E, Santos JL, Centeno MA, Arellano-Garcia H, et al. Chemical CO2 recycling via dry and bi reforming of methane using Ni-Sn/Al2O3 and Ni-Sn/CeO2-Al2O3 catalysts. Appl. Catal. B Environ. 2018;224:125–35. https://doi.org/10.1016/j.apcatb.2017.10.047.

[39] Le Saché E, Santos JL, Smith TJ, Centeno MA, Arellano-Garcia H, Odriozola JA, et al. Multicomponent Ni-CeO2 nanocatalysts for syngas production from CO2/CH4 mixtures. J CO2 Util 2018;25:68–78. https://doi.org/10.1016/j.jcou.2018.03.012.

[40] Wang L, Zhang S, Liu Y. Reverse water gas shift reaction over Co-precipitated Ni-CeO2 catalysts. J Rare Earths 2008;26:66–70. https://doi.org/10.1016/S1002-0721(08)60039-3.

[41] Zonetti PC, Letichevsky S, Gaspar AB, Sousa-Aguiar EF, Appel LG. The NixCe0.75Zr0.25-xO2 solid solution and the RWGS. Appl Catal A Gen 2014;475: 48–54. https://doi.org/10.1016/j.apcata.2014.01.004.

[42] Yang L, Pastor-Pérez L, Gu S, Sepúlveda-Escribano A, Reina TR. Highly efficient Ni/CeO2-Al2O3 catalysts for CO2 upgrading via reverse water-gas shift: effect of selected transition metal promoters. Appl Catal B Environ 2018;232:464–71. https://doi.org/10.1016/j.apcatb.2018.03.091.

[43] Cai M, Wen J, Chu W, Cheng X, Li Z. Methanation of carbon dioxide on Ni/ZrO2-Al2O 3 catalysts: effects of ZrO2 promoter and preparation method of novel ZrO2-Al2O3 carrier. J Nat Gas Chem 2011;20:318–24. https://doi.org/10.1016/S1003-9953(10)60187-9.

[44] Pan Q, Peng J, Sun T, Gao D, Wang S, Wang S. CO2 methanation on Ni/Ce0.5Zr0.5O 2 catalysts for the production of synthetic natural gas. Fuel Process Technol 2014;123:166–71. https://doi.org/10.1016/j.fuproc.2014.01.004.

[45] Ocampo F, Louis B, Kiwi-Minsker L, Roger AC. Effect of Ce/Zr composition and noble metal promotion on nickel based CexZr1-xO2 catalysts for carbon dioxide methanation. Appl. Catal. A Gen. 2011;392:36–44. https://doi.org/10.1016/j.apcata.2010.10.025.

[46] Trimm DL. Coke formation and minimisation during steam reforming reactions. Catal Today 1997;37:233–8. https://doi.org/10.1016/S0920-5861(97)00014-X.

[47] Nagaoka K, Seshan K, Lercher JA, Aika KI. Activation mechanism of methane-derived coke (CHx) by CO2 during dry reforming of methane - comparison for Pt/Al2O3 and Pt/ZrO2. Catal. Letters. 2000;70:109–16. https://doi.org/10.1023/A:1018877032022.

[48] Solymosi F, Kutsán G, Erdöhelyi A. Catalytic reaction of CH4 with CO2 over alumina-supported Pt metals. Catal Lett 1991;11:149–56. https://doi.org/10.1007/BF00764080.

[49] Porosoff MD, Chen JG. Trends in the catalytic reduction of CO2 by hydrogen over supported monometallic and bimetallic catalysts. J Catal 2013;301:30–7. https://doi.org/10.1016/j.jcat.2013.01.022.

[50] Kim SS, Lee HH, Hong SC. A study on the effect of support's reducibility on the reverse water-gas shift reaction over Pt catalysts. Appl Catal A Gen 2012;423–424: 100–7. https://doi.org/10.1016/j.apcata.2012.02.021.

[51] Kwak JH, Kovarik L, Szanyi J. Heterogeneous catalysis on atomically dispersed supported metals: CO 2 reduction on multifunctional Pd catalysts. ACS Catal 2013; 3:2094–100. https://doi.org/10.1021/cs4001392.

[52] Kwak JH, Kovarik L, Szanyi J. CO2 reduction on supported Ru/Al2O3 catalysts: cluster size dependence of product selectivity. ACS Catal 2013;3:2449–55. https://doi.org/10.1021/cs400381f.

[53] Gao J, Liu Q, Gu F, Liu B, Zhong Z, Su F. Recent advances in methanation catalysts for the production of synthetic natural gas. RSC Adv 2015;5:22759–76. https://doi.org/10.1039/c4ra16114a.

[54] Duyar MS, Wang S, Arellano-Treviño MA, Farrauto RJ. CO2 utilization with a novel dual function material (DFM) for capture and catalytic conversion to synthetic natural gas: an update. J CO2 Util 2016;15:65–71. https://doi.org/10.1016/j.jcou.2016.05.003.

[55] Valdés-Martínez OU, Suárez-Toriello VA, los Reyes JAd, Pawelec B, Fierro JLG, Support effect and metals interactions for NiRu/Al2O3, TiO2 and ZrO2 catalysts in the hydrodeoxygenation of phenol. Catal Today 2017; 296: 219–27. https://doi.org/10.1016/j.cattod.2017.04.007.

[56] Crisafulli C, Scirè S, Minicò S, Solarino L. Ni-Ru bimetallic catalysts for the CO2 reforming of methane. Appl Catal A Gen 2002;225:1–9. https://doi.org/10.1016/S0926-860X(01)00585-3.

[57] Wang S, Lu GQ. Role of CeO2 in Ni/CeO2-Al2O3 catalysts for carbon dioxide reforming of methane. Appl Catal B Environ 1998;19:267–77. https://doi.org/10.1016/S0926-3373(98)00081-2.

[58] Liu Y, Li Z, Xu H, Han Y. Reverse water-gas shift reaction over ceria nanocube synthesized by hydrothermal method. Catal Commun 2016;76:1–6. https://doi.org/10.1016/j.catcom.2015.12.011.

[59] Tada S, Ochieng OJ, Kikuchi R, Haneda T, Kameyama H. Promotion of CO2 methanation activity and CH4 selectivity at low temperatures over Ru/CeO2/Al2O 3 catalysts. Int J Hydrogen Energy 2014;39:10090–100. https://doi.org/10.1016/j.ijhydene.2014.04.133.

[60] Liu H, Zou X, Wang X, Lu X, Ding W. Effect of CeO2 addition on Ni/Al2O3 catalysts for methanation of carbon dioxide with hydrogen. J Nat Gas Chem 2012;21:703–7. https://doi.org/10.1016/S1003-9953(11)60422-2.

[61] Trovarelli A, Boaro M, Rocchini E, De Leitenburg C, Dolcetti G. Some recent developments in the characterization of ceria-based catalysts. J Alloy Compd 2001; 323–324:584–91. https://doi.org/10.1016/S0925-8388(01)01181-1.

[62] Li M, Amari H, van Veen AC. Metal-oxide interaction enhanced CO2 activation in methanation over ceria supported nickel nanocrystallites. Appl Catal B Environ 2018;239:27–35. https://doi.org/10.1016/j.apcatb.2018.07.074.

[63] Bereketidou OA, Goula MA. Biogas reforming for syngas production over nickel supported on ceria-alumina catalysts. Catal Today 2012;195:93–100. https://doi.org/10.1016/j.cattod.2012.07.006.

[64] Le Saché E, Johnson S, Pastor-Pérez L, Horri BA, Reina TR. Biogas upgrading via dry reforming over a Ni-Sn/CeO2-Al2O3 catalyst: influence of the biogas source. Energies 2019;12. https://doi.org/10.3390/en12061007.

[65] Pastor-Pérez L, Baibars F, Le Sache E, Arellano-García H, Gu S, Reina TR. CO2 valorisation via reverse water-gas shift reaction using advanced Cs doped Fe-Cu/Al2O3 catalysts. J CO2 Util 2017;21:423–8. https://doi.org/10.1016/j.jcou.2017.08.009.

[66] Chen X, Su X, Duan H, Liang B, Huang Y, Zhang T. Catalytic performance of the Pt/TiO2 catalysts in reverse water gas shift reaction: controlled product selectivity and a mechanism study. Catal Today 2017;281:312–8. https://doi.org/10.1016/j.cattod.2016.03.020.

[67] Zhang Z, Tian Y, Zhang L, Hu S, Xiang J, Wang Y, et al. Impacts of nickel loading on properties, catalytic behaviors of Ni/Γ–Al 2 O 3 catalysts and the reaction intermediates formed in methanation of CO 2. Int J Hydrogen Energy 2019;44: 9291–306. https://doi.org/10.1016/j.ijhydene.2019.02.129.

[68] Tao K, Shi L, Ma Q, Wang D, Zeng C, Kong C, Wu M, Chen L, Zhou S, Hu Y, Tsubaki N, Methane reforming with carbon dioxide over mesoporous nickel-alumina composite catalys. Chem Eng J 2013; 221: 25–31. https://doi.org/10.1016/j.cej.2013.01.073.

[69] Pastor-Pérez L, Sepúlveda-Escribano A. Multicomponent NiSnCeO2/C catalysts for the low-temperature glycerol steam reforming. Appl Catal A Gen 2017;529: 118–26. https://doi.org/10.1016/j.apcata.2016.10.022.

[70] Pastor-Perez L, Buitrago-sierra R, Sepulveda-Escribano A. CeO2-promoted Ni/activated carbon catalysts for the water-gas shift (WGS reaction. Int J Hydrogen Energy 2014;9:17589–99. https://doi.org/10.1016/j.ijhydene.2014.08.089.

[71] Meloni E, Martino M, Palma V. A short review on ni based catalysts and related engineering issues for methane steam reforming. Catalysts 2020;10. https://doi.org/10.3390/catal10030352.

[72] Mierczynski P, Stępińska N, Mosinska M, Chalupka K, Albinska J, Maniukiewicz W, et al. Hydrogen production via the oxy-steam reforming of lng or methane on ni catalysts. Catalysts 2020;10. https://doi.org/10.3390/catal10030346.

[73] Prakash AS, Shivakumara C, Hegde MS. Single step preparation of CeO2/CeAlO3/γ-Al2O3 by solution combustion method: Phase evolution, thermal stability and surface modification. Mater Sci Eng B Solid-State Mater Adv Technol 2007;139: 55–61. https://doi.org/10.1016/j.mseb.2007.01.034.

[74] Bradford MCJ, Vannice MA. CO2 reforming of CH4. Catal Rev - Sci Eng 1999;41: 1–42. https://doi.org/10.1081/CR-100101948.

[75] Choudhary VR, Rajput AM. Simultaneous carbon dioxide and steam reforming of methane to syngas over NiO-CaO catalyst. Ind Eng Chem Res 1996;35:3934–9. https://doi.org/10.1021/ie960002l.

[76] Mebrahtu C, Krebs F, Perathoner S, Abate S, Centi G, Palkovits R. Hydrotalcite based Ni-Fe/(Mg, Al)O: X catalysts for CO2 methanation-tailoring Fe content for improved CO dissociation, basicity, and particle size. Catal Sci Technol 2018;8: 1016–27. https://doi.org/10.1039/c7cy02099f.

[77] Rynkowski JM, Paryjczak T, Lewicki A, Szynkowska MI, Maniecki TP, Jóźwiak WK. Characterization of Ru/CeO2-Al2O3 catalysts and their performance in CO2 methanation. React Kinet Catal Lett 2000;71:55–64. https://doi.org/10.1023/A:1010326031095.

[78] Lavoie JM. Review on dry reforming of methane, a potentially more environmentally-friendly approach to the increasing natural gas exploitation. Front Chem 2014;2:1–17. https://doi.org/10.3389/fchem.2014.00081.

[79] Bartholemew CH, Model catalyst studies of supported metal sintering and redispersion kinetics, in: Catal. Vol. 10, Royal Society of Chemistry, 1993: 41–82. https://doi.org/10.1039/9781847553225-00041.